Biophysical Journal Volume 103 July 2012 99–108

Folding a Protein with Equal Probability of Being Helix or Hairpin

Chun-Yu Lin,[†] Nan-Yow Chen,[‡] and Chung Yu Mou[†§¶*]
[†]Department of Physics, National Tsing Hua University, Hsinchu, Taiwan; [‡]National Center for High-Performance Computing, Hsinchu, Taiwan; [§]Institute of Physics, Academia Sinica, Nankang, Taiwan; and [¶]Physics Division, National Center for Theoretical Sciences, Hsinchu, Taiwan

ABSTRACT We explore the possibility for the native structure of a protein being inherently multiconformational in an ab initio coarse-grained model. Based on the Wang-Landau algorithm, the complete free energy landscape for the designed sequence 2DX4: INYWLAHAKAGYIVHWTA is constructed. It is shown that 2DX4 possesses two nearly degenerate native structures: one is a helix structure with the other a hairpinlike structure, and their free energy difference is $<2\%$ of that of local minima. Two degenerate native structures are stabilized by an energy barrier of ~10 kcal/mol. Furthermore, the hydrogen-bond and dipole-dipole interactions are found to be two major competing interactions in transforming one conformation into the other. Our results indicate that two degenerate native structures are stabilized by subtle balance between different interactions in proteins. In particular, for small proteins, balance between the hydrogen-bond and dipole-dipole interactions happens for proteins of sizes being ~18 amino acids and is shown to the main driving mechanism for the occurrence of degeneracy. These results provide important clues to the study of native structures of proteins.

INTRODUCTION

Solving the protein-folding problem has tremendous implications. Among possible applications, the solution to the problem makes it possible to design drugs theoretically, which would result in the greatest impact to the biological science. Nonetheless, despite much effort being devoted during the past, the problem continues to be one of the most basic unsolved problems. To solve the folding problem completely, it is generally believed that to be able to predict the protein structure for a given sequence of amino acids is the key step. Following the classical Anfinsen's work (1), it is known that the native state of a globular protein would lie at the minimum of the free energy; hence, the problem of structure prediction reduces to the problem of finding the minimum of the free energy.

During the past decades, it has become evident that the free energy landscape for a given segment of amino acids is more complicated than was previously thought and may possess local minima exhibited as metastable states. Such evidence has been often exhibited as the conformation switch of proteins. For instance, the bovine β-lactoglobulin protein is a predominantly β-sheet protein but it has been observed to go through a remarkable $\alpha \rightarrow \beta$ transition during the folding process (2,3). In the effort of unraveling the mechanism for protein misfolding and aggregation, which are known to be causes for perplexing diseases such as Alzheimer's disease and the prion encephalopathies, it is found that even though aggregates found in the patients of Alzheimer's disease comprise extended β-sheet structures, the building block of the aggregates (the amyloid-β monomer) adopts a random coil structure in aqueous solution (4,5) or predominantly α-helix structure in membrane-mimicking environments (6,7). It is thus rational to postulate that an $\alpha \rightarrow \beta$ or a random coil $\rightarrow \beta$ transition occurs during the early aggregation process (8).

Typically, a conformation switch of proteins can be induced by changing external conditions such as the pH value, the ionic strength (9,10), the temperature (11), the solvent polarity (12), or by mutating a few amino acids. Kabsch and Sander (13) found a pentapeptide sequence that could adopt an α-helix or a β-sheet conformation in different proteins. Cohen et al. (14) extended this work to hexapeptides. Minor and Kim (15) have conducted an experiment showing that an 11-amino-acid sequence can be transformed into an α-helix or a β-sheet in protein G. Such chameleon-like sequences have their cooperative local interactions competing against long-range interactions of sequence environment. The fragmental propensity of secondary structures is found to be overwhelmed by larger structures. It is also shown that proteins may evolve from one structure to another by mutating single or several amino acids in sequence (16,17). The general assumption behind this is that the key mutation would destabilize the original structure, and favor another propensity.

The above facts indicate that there may exist nearby competing states to the native state of a given protein. Therefore, given appropriate conditions, the native state of a given sequence of amino acids can be changed. To elucidate the real mechanism that causes the conformation change, a de novo protein has recently been designed by Araki and Tamura (18). They reported a modified sequence INYWLAHAKAGYIVHWTA deposited in the Protein Data Bank (19) (PDB IDs 2DX3 and 2DX4; we shall term this simply as 2DX4 hereafter) was identified to have equal populations of α-helical or β-sheet in an aqueous solution.

Submitted November 28, 2011, and accepted for publication May 17, 2012.
*Correspondence: mou@phys.nthu.edu.tw
Editor: Michael Levitt.

0006-3495/12/07/0099/10 $2.00
doi: 10.1016/j.bpj.2012.05.029

Although it is well recognized that protein solutions are in equilibrium with intermediate peptides, the dual native structures are rarely reported in the literature. Furthermore, it is shown that the conformational transformation of 2DX4 is not induced by any environmental conditions or binding motifs. These facts make 2DX4 a valuable target to study. In particular, folding 2DX4 would be a crucial test for any viable approach for solving the protein-folding problem.

On the theoretical side, all-atom simulation is the most comprehensive approach for understanding the folding processes; however, the requirement of computational resources tends to be realistically unaffordable (20). Itoh et al. (21) have combined all-atom molecular-dynamics simulation with multicanonical multioverlap algorithm to simulate 2DX4. From the limited phase space obtained, they investigated possible pathways for the $\alpha \rightarrow \beta$ transition. In particular, three local minima in free energy are identified. However, only partial α-helices or β-hairpins are found in the structures associated with these local minima. The mechanism that is responsible for the possibility of two native structures of 2DX4 thus remains unclear. On the other hand, there has been much effort in developing coarse-grained models to predict protein structures (22). In these models, effects of water molecules are implicitly included in effective interacting potentials between amino acids. The required computational resources are much reduced and it enables the prediction of protein structures feasible. Indeed, progress have recently been made in predicting structures of wild-type proteins of sizes from 12 to 56 amino acids by using realistic and unbiased potentials between amino acids (23). To further check the validity of coarse-grained models, folding proteins such as 2DX4 would be an ideal test.

In this work, based on an ab initio coarse-grained model constructed in Chen et al. (23), we constructed the complete free energy landscape for 2DX4. It is shown that in agreement with the experimental observation, there are only two native structures associated with local minima of the free energy: α-helix- and β-hairpin-like structures. Moreover, within the accuracy of the coarse-grained model, it is found that whereas local minima are degenerate in the case of 2DX4, the β-hairpin-like structure is higher in energy for the DP3 protein that results from the mutation of one amino acid of 2DX4 and was reported to have zero population of hairpin structure (18). In addition, the pathways between the helix and hairpin configurations are simulated by Monte Carlo (MC) algorithm in high temperatures. By analyzing a detailed free-energy profile, we find that the hydrogen-bond and dipole-dipole interactions are two major competing mechanisms in transforming one conformation into the other. Our results indicate that, generally, degenerate native structures are stabilized by subtle balance between different interactions in proteins. For small proteins, the balance between the hydrogen-bond and dipole-dipole interactions can occur for sizes of proteins being ~18 amino acids or 40 amino acids. These results provide important clues to the study of the native structures of proteins.

THEORY AND METHODS

Ab initio coarse-grained potentials

We shall first recapture essentials of the coarse-grained model constructed in Chen et al. (23). In this model, residues are coarse-grained, as spheres are centered at C^{β} atoms but complete structures are kept in backbones. Bond angles and bond lengths are fixed between these atoms to increase folding efficiency; the only variables are dihedral angles φ and ψ on the C^{α} atom-hinging, two-amide planes. Water molecules are not included explicitly, but their effects are incorporated in effective potentials among side chains and backbones. In these representations and with all energies being in unit of kcal/mol, the total energy can be written as

$$E_{total} = E_{Steric} + E_{DD} + E_{HB} + E_{MJ} + E_{NP} + E_{SA}. \quad (1)$$

Here each energy term is a weighted potential energy with $E_i = \epsilon_i V_i$, where ϵ_i is the weighting factor to be determined later and V_i is the corresponding potential energy. Among these energy terms, E_{Steric} is to enforce the structural constraints such as hard-core potentials to avoid unphysical contacts, whereas E_{SA} is the solvent-accessible surface energy in proportion to the area of each side chain that is exposed to water and is primarily responsible for stabilizing the tertiary structure. The remaining terms are three ingredients for the formation of the secondary structures, with E_{HB} being the hydrogen-bonding between any nonneighboring NH and CO pair, E_{DD} being the summation of screened dipole-dipole interaction at large distance (global dipole interaction, E_{DG}) and local dipole-dipole interaction between dipoles on the backbones, and $E_{MJ} + E_{NP}$ accounting for the interactions due to hydrophobicity or the charge state of the amino acids. Except for $E_{MJ} + E_{NP}$, all the potentials are based on realistic and bare values of parameters obtained from experimental data. The potential, $E_{MJ} + E_{NP}$, was based on simple generalizations of the Miyazawa-Jernigan matrix (24,25) by using a 12-6 Lennard-Jones potential modified by effects due to the sizes of water molecules (23). To include realistic effects due to hydrophobicity or the charge state of the amino acids, we shall construct the corresponding potentials by statistical methods so that E_{MJ} generalizes the Miyazawa-Jernigan matrix (24,25) to finite large distances between amino acids, whereas E_{NP} generalizes the $V_{LocalHP}$ in Chen et al. (23) and is the statistical energy that characterizes the propensity (to α or β) of amino acids in nearest neighbors.

With these potentials, the weighting factor values ϵ_i are calibrated based on a few proteins of known structures (22). Details of calibration are given in the next subsection. Typical values of ϵ_i are $\epsilon_{DG} = 0.21$, $\epsilon_{DN} = 2.0$, $\epsilon_{HB} = 4.8$, $\epsilon_{SA} = 1.35$, and $\epsilon_{MJ} = 0.85$. For helix and sheet propensity energies, we get $\epsilon_{NP}^{\alpha} = 6.4$ and $\epsilon_{NP}^{\beta} = 16$. These calibrated parameters are then used to fold various target proteins. Note that there are ranges of parameters that allow successful folding of target proteins. In our model, success of folding target proteins requires a strong hydrogen-bonding: the upper bound of a hydrogen bound is 4.8 kcal/mol (the magnitude of the hydrogen bond by taking the vacuum as a reference point); the lower bound of the energy for the hydrogen bond is 3.84 kcal/mol. The lower bound is larger than the value of 3.1 kcal/mol obtained in careful studies of the hydrogen bond (26,27).

For ordered states, because it is the relative strengths between different energy terms that determine the native structures, relative ratios of energy terms are more important. These ratios are fixed by calibrating the weighting factor ϵ_i. In the allowed ranges of parameters, the lower bound of the ratio of the hydrogen bond to a typical bonding in E_{MJ} (taking the interaction between Leu and Leu as an example) is $3.84/1.02 = 3.77$, which is about the same scale as $3.44 (= 3.1/0.9)$ that was adopted in the literature

(26). Therefore, even though the absolute magnitude of the hydrogen bond used is strong, the lower bounds of relative strengths of the hydrogen bond to other energy terms are about the same scales adopted in the literature.

To extend the Miyazawa-Jernigan matrix to finite distances, we perform extended statistical analysis by first writing

$$E_{MJ} = \epsilon_{MJ} \sum_{i,j} V_{ij;MJ}(r)(1 - SA_i)\big(1 - SA_j\big), \qquad (2)$$

where SA_i and SA_j are the solvent accessibilities for i^{th} and j^{th} residues, respectively. The quantity, $V_{ij;MJ}(r)$, is the statistical potential between the i^{th} and j^{th} residues obtained by counting number n_{ij}, of the corresponding i-type and j-type residues separating by r, that appears in the PDB. Fundamentally, $V_{ij;MJ}(r)$ is the generalization of the pair distribution function (28) and its relation to $n_{ij}(r)$ is given by the Boltzmann's statistics

$$\exp\big(-V_{ij;MJ}(r)\big) = A(r_k) \frac{\sum_p n_{ij;p}(r_k)}{\sum_{p,r_k} \frac{\big(n_{ir;p}(r_k) + n_{i0;p}(r_k)\big)\big(n_{jr;p}(r_k) + n_{j0;p}(r_k)\big)}{\big(n_{rr;p}(r_k) + n_{r0;p}(r_k)\big)}}, \qquad (3)$$

where $A(r_k)$ is a normalization factor to be determined later, numbers with the index p denote the corresponding statistical values that belong to one specific protein p, 0 represents the solvent group, and r_k is the radius of the k^{th} spherical shell centered at i-type residue. Note that different amino acids have a different occurrence frequency in real proteins and this is normalized by the denominator in Eq. 3. Furthermore, homology of sequence bias was eliminated by the sequence alignment method in combination with the weighting matrix used by Miyazawa and Jernigan (25). Here $2n_{ij}(r_k)$ for $i \neq j$ and $n_{ij}(r_k)$ are the counts when the i-type residue is at the origin and the j-type residue is in the k^{th} distance r_k, whereas n_{ir} is the total count of the i^{th} residue

$$n_{ir;p}(r_k) = \sum_j n_{ij;p}(r_k). \qquad (4)$$

The value n_{i0} counts events taking place between the i-type residue and solvent group 0,

$$n_{i0;p}(r_k) = \frac{1}{2} q_i(r_k) n_{i;p}(r_k) - n_{ir;p}(r_k), \qquad (5)$$

where q_i is the coordinate number of the i-type residue in the k^{th} spherical shell and n_i is the total number of the i-type residues in protein p. The values n_{rr} and n_{r0} are summations of n_{ir} and n_{i0} over i-type residue, respectively,

$$n_{rr;p}(r_k) = \sum_i n_{ir;p}(r_k), \qquad (6)$$

$$n_{0r;p}(r_k) = \sum_i n_{i0;p}(r_k). \qquad (7)$$

Finally, the normalization factor $A(r)$ is defined by

$$A(r_k) = \frac{\text{total number of shells}}{\frac{4}{3}\pi\left[\left(r_k + \frac{\Delta r}{2}\right)^3 - \left(r_k - \frac{\Delta r}{2}\right)^3\right]}, \qquad (8)$$

where Δr is the width of each spherical shell. The effective potential as a continuous function of r, $V_{ij;MJ}(r)$ is then interpolated from $V_{ij;MJ}(r_k)$. As a demonstration, in Fig. 1, we show a typical effective potential obtained by the above statistical analysis. We see that similar to the pair-distribution function for liquid molecules (28), $V_{ij;MJ}(r)$ exhibits oscillations similar to those of the desolvation model (29). Clearly, an energy barrier exists before two amino acids get closer to the repulsive core. The desolvation-like barrier was not included in many implicit-solvent potentials (30). However, it has been pointed out that the barrier favors the β-sheet rather than the α-helix and may play significant roles in the formation of secondary structure (31). Note that the origin of the energy barrier shown in Fig. 1 is not purely contributed by solvent molecules, thus it is different from the desolvation mechanism. Nevertheless, the insertion of effective solvent groups (defined by Miyazawa and Jernigan (24) and utilized here) cooperating with residue contacts can represent an effective liquid-phase potential.

In the linear regression analysis of $V_{ij;MJ}(r)$, the correlation of the first and the second minimum positions r_1 and r_2 is 0.925 and can be represented by

$$r_2 = 1.21 r_1 + 0.34\big(l_{sc,i} + l_{sc,j}\big) + a_0.$$

Here r_1 is found to be the summation of averaged radius of residues i and j, $r_1 = a_i + a_j$, $l_{sc,i}$ is the maximum excess length of residue i over the averaged radius (ranges from 1 to 5), and $a_0 = 1.61$ Å is the size of an effective solvent molecule. Furthermore, even though there are structures in proteins, there is no indication of any ordering in $V_{ij;MJ}(r)$. The effective $V_{ij;MJ}(r)$ is only valid for large enough distances. For residues in nearest neighbors, due to the steric constraints, the pair distribution function starts to deviate from the desolvation model. To extend E_{MJ} to characterize interactions of residues in nearest neighbors, E_{NP} is introduced to account for the statistical energy between nearest-neighboring residues. The interactions among nearest-neighboring residues are best characterized by dihedral angles ϕ and ψ of the corresponding amide planes. Because $V_{ij;MJ}(r)$ does not cover distances of three successive residues, E_{NP} needs to characterize

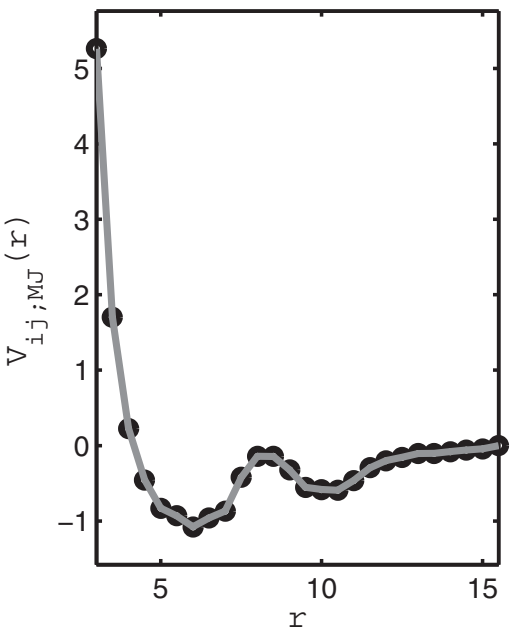

FIGURE 1 A typical effective potential, $V_{ij;MJ}(r)$. Here the potential is between Valine and Leucine. (*Solid line*) Continuous curve interpolated between data obtained by statistical analysis of PDB. One sees that even though there are structures in proteins, $V_{ij;MJ}(r)$ shows liquidlike behavior and exhibits oscillations similar to those exhibited in the desolvation model.

three successive residues in the protein, labeled by $i-1$, i, and $i+1$. Using the corresponding dihedral angles shown in Fig. 2 *a*, E_{NP} can be written as

$$E_{NP} = \sum_i \sum_{k=\alpha,\beta} \varepsilon_{NP}^k \left[V_{lm}^k(\psi_{i-1},\phi_i) + V_{mn}^k(\psi_i,\phi_{i+1})\right] \times V_m(\phi_i,\psi_i), \quad (9)$$

where l, m, and n are indices for type of residues, V_m is a one-body potential that depends on ψ_i and ϕ_i of the amide planes connecting to the m-type residue, and V_{lm} (also V_{mn}) is a two-body energy that depends on dihedral angles of l-type and m-type residues in nearest neighbors. According to the Ramachandran plot, it is known that ϕ and ψ are statistically concentrated at particular regions, which are either in the α-helix configuration or β-sheet configuration. To ensure the relative magnitudes of α-helix and β-sheet part are not biased by the database, different weighting factors with $k = \alpha$ and β are introduced in Eq. 9. The one-body angular potential V_m is obtained by first analyzing the bare potential v_m, defined by

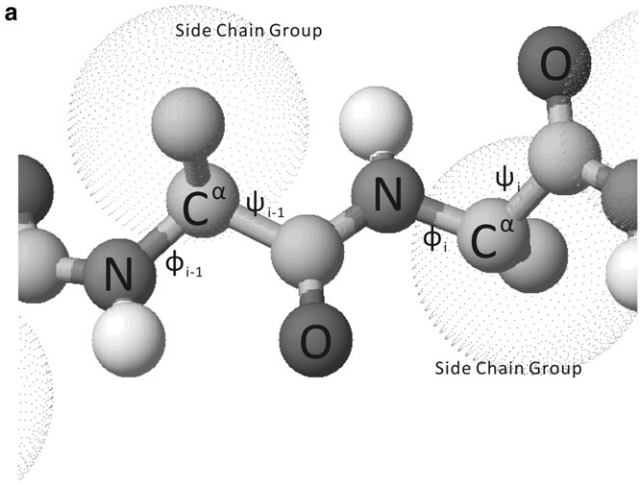

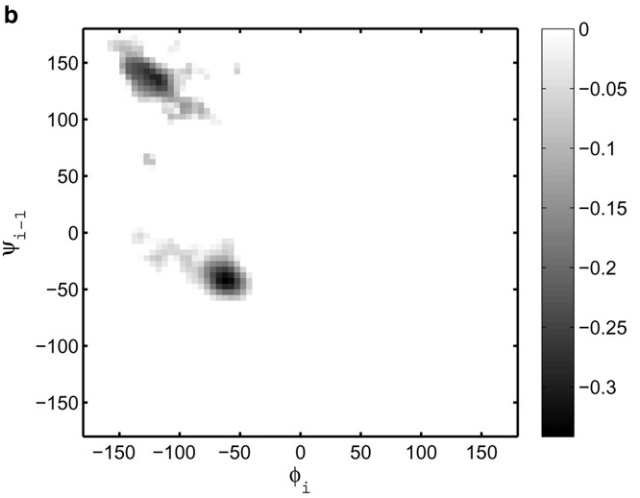

FIGURE 2 (*a*) Dihedral angles that characterize effective potentials for nearest-neighboring residues. (*b*) A typical effective potential, $V_{i-1,i}^{\alpha} + V_{i-1,i}^{\beta}$, between nearest-neighboring amino acids. Here the interaction is between the Aspartic acid and Tyrosin. Similar to the Ramachandran plot, the potential is significant only in the regions with α- or β-structures.

$$\exp(-v_m(\phi,\psi)) = \frac{n_m(\phi,\psi)}{\iint n_m(\phi,\psi)d\phi d\psi}, \quad (10)$$

where n_m is the number density taken over the whole PDB for type-m residues with dihedral angles being (ϕ,ψ). To account for the preference or nonpreference of α- or β-structures, we set

$$V_m(\phi_i,\psi_i) = \theta(\Lambda - v_m(\phi_i,\psi_i)),$$

with θ being the step function and Λ being a negative threshold energy level so that V_m is either 1 or 0.

The bare two-body potential is constructed by

$$\exp\left(-v_{lm}^k(\psi_{i-1},\phi_i)\right) = \frac{n_{lm}(\psi_{i-1},\phi_i)\iint n_{rr}(\psi_{i-1},\phi_i)d\psi_{i-1}d\phi_i}{\iint n_{lr}(\psi_{i-1},\phi_i)d\psi_{i-1}d\phi_i \iint n_{mr}(\psi_{i-1},\phi_i)d\psi_{i-1}d\phi_i}, \quad (11)$$

where n_{lr}, n_{mr}, and n_{rr} are defined in same way as those in Eqs. 4 and 6, except that they are specialized to the dihedral angle (ψ_{i-1}, ϕ_i). The expression $V_{lm}^k(\psi_{i-1},\phi_i)$ is then defined by rescaling v_{lm} with respect to the average value of v_{lm},

$$V_{lm}^k(\psi_{i-1},\phi_i) = \frac{\left(A_{lm}^k - A_{ave}^k\right)v_{lm}^k(\psi_{i-1},\phi_i)}{A_{lm}^k}, \quad (12)$$

where A_{lm} is the minimum of v_{lm} over all possible (ψ_{i-1}, ϕ_i) values and A_{ave} is the average value of A_{lm} over all possible pairs of amino acids. A typical V_{lm} is shown in Fig. 2 *b*. It is clear that $V_{i-1,i}(\psi_{i-1}, \phi_i)$ does not vanish only in particular regions, in which local structures of proteins are either α-helices or β-sheets.

Calibration of energy weighting factors

The weighting factors ϵ_i are calibrated by comprehensively searching valid values within specific ranges in a selected set of reference proteins, which are 1NJ0, 1DJF, 1GB4, 1PIQ, and 2NOU. Specifically, a set of decoy conformations of the reference proteins is selected and the weighting factors have to be in the physical region in which total energies of decoy conformations are greater than those of native structures. To adjust the weighting factors toward the physical region, a cost function is defined by

$$cost = \frac{\sum_i \Delta E_{total} \cdot D_i^{RMS} \cdot f_i}{\sum_i D_i^{RMS} \cdot f_i}. \quad (13)$$

Here $\Delta E_{total} = E_{total}^i - E_{total}^{i,native}$ with i being the index for the decoy configuration and $E_{total}^{i,native}$ being the total energy of the native state for the corresponding reference protein. The factor f_i gives high score to the negative values so that weighting factors in the unphysical region can be identified: $f_i = 1$ for $\Delta E_{total} > 0$, otherwise $f_i = \epsilon/(1 + \Delta E^2_{total})$ with ϵ being an arbitrary small number chosen as 10^{-8}. D_i^{RMS} measures deviation of the decoy conformation from the native structures and is the relative root mean-square distance defined by Betancourt and Skolnick (32). The set of weighting factors that corresponds to the most positive cost value will be selected. The optimization results and allowed ranges of weighting factors are listed in Table 1. Changing one factor from the default value within the allowed range will not cause serious misfolding. For efficiency, only five reference proteins are used for optimization. Furthermore, during the calibration, if the reference proteins end up with any wrong conformations, in the newly launched Monte Carlo simulation with the selected factors, the misfolded

TABLE 1 Weighting factors of energy terms and its valid range

	Default	Lower limit	Upper limit
ϵ_{DG}	0.21	0.00	2.56
ϵ_{DN}	2.00	2.00	2.60
ϵ_{HB}	4.80	3.84	4.80
ϵ_{NP}^{α}	6.40	4.48	8.32
ϵ_{NP}^{β}	16.0	14.4	19.2
ϵ_{MJ}	0.85	0.43	1.45
ϵ_{SA}	0.35	0.54	3.78

conformations will be added into the decoy sets and rerun the process iteratively.

Although the reference proteins are not plentiful, the emerged weighting factors will be examined further by folding a larger pool of target proteins. These targets comprise secondary structures of α-helix (PDB ID: 1DJF, 1DN3, 1DNG, 1DU1, 1EMZ, 1EQX, 1FAC, 1GJF, 1HU6, 1JZP, 1KYC, 1KZ2, 1LBJ, 1O53, 1ODP, 1ODQ, 1QG9, 1XOO, 1XOP, 2A1C, 2AP7, 2B0Y, 2BBL, 2DCI, 2FQ5, 2FXY, 2I9M, 2JMY, 2JOF, 2RLG, 2RLH, and 1S4W); β-sheet (1B03, 1E0Q, 1E0N, 1J4M, 1K43, 1U6U, 2ESZ, 2ORU, and 1NJ0); and mixed α/β structures (1FSV, 1PSV). At the end, all the target proteins are correctly folded.

Wang-Landau Monte Carlo algorithm

Given the ab initio coarse-grained potential obtained, one can determine the free energy landscape by using the Wang-Landau algorithm (33). The density of states is estimated by random sampling on energy space via the transition probability

$$P(E_1 \rightarrow E_2) = \min\left(\frac{g(E_1)}{g(E_2)}, 1\right), \tag{14}$$

where $g(E)$ is the density function of energy E. Although this algorithm was first demonstrated on Ising model of spin array, it is portable to molecular systems with continuous energy value (34,35). Specific implementations adapted in our work are the following steps:

1. Define a density function $g(E, X)$ and histogram $H(E, X)$ with X values being any variables other than energy. Set initial values: $g(E, X) = 1$ and $H(E, X) = 0$ for all E and X.
2. Generate an initial conformation randomly and calculate its energy E_1.
3. Generate a new conformation by making a small change (e.g., the dihedral angles). Calculate the new energy E_2, and the transition to the new conformation is determined by the transition probability $P(E_1, X_1 > E_2, X_2) = \min[g(E_1, X_1)/g(E_2, X_2)1]$.
4. If the system stays in the original E_1 state, $g(E_1, X_1)$ is replaced by $g(E_1, X_1) \times f$ and $H(E, X)$ is accumulated through $H(E_1, X_1) + 1$. Otherwise, one sets $g(E_2, X_2) = g(E_2, X_2) \times f$ and $H(E_2, X_2) = H(E_2, X_2) + 1$. The factor f is initially set to e_1.
5. After each MC step, check if $<2\%$ of sites in H are smaller than flat threshold, which is defined to be 10% of averaged $H(E, X)$. If this is satisfied, the histogram is flat and one then sets $f = \sqrt{f}, H(E, X) = 0$ and goes to Step 2. When $f < \exp(10^{-3.6})$ is satisfied, one exits the procedure.

All the above steps are identical to Wang-Landau's scheme except for the flat histogram criteria in Step 5, which is modified to accommodate enormous states involved for proteins so that sampling can be done in finite computation time. Once the density of states is constructed, the free energy landscape can be calculated as

$$F(E, X) = E - k_B T \log[g(E, X)], \tag{15}$$

where k_B is the Boltzmann constant and T is the absolute temperature. The variable space X is not restricted to be one dimension and has to be chosen to exhibit the landscape.

RESULTS

Propensity analysis and Monte Carlo simulation

To investigate the energy landscape of 2DX4, we first analyze its propensity. Past studies (36,37) have indicated that each amino acid has its propensity of secondary structure. By using the constructed statistical potential V_{lm} (see Theory and Methods), we summarize the nearest-neighbor propensity of 2DX4 in Fig. 3. Here amino acids in nearest neighbors are classified according to the tendency of corresponding amino acids being in α-helix, β-sheet, dual, or neutral. The dual propensity implies the residue pair can adopt either α- or β-structure. By contrast, the neutral propensity implies that the residue pair is free to rotate in dihedral angles and it is often that a turn region of antiparallel β-sheet is developed. From the propensity analysis, it is clear that even though there is no absolute global tendency for 2DX4 being α-helix or β-sheet, by including residues with neutral and dual propensities, there are more residues in favor of α-helix. Nonetheless, the high β-sheet propensity near the C-terminal, containing amino acids V, H, and W, indicates the possibility of switching 2DX4 between helix and hairpin structures. Because each of these three amino acids has larger side-chain radius than the averaged radius of others, it is more difficult for the segment to curl into part of the helix structure. As a result, the strand formed by residues 14–18 regularly dangles in solvent and deposits a nucleation seed to transform from α-helix to β-sheet.

To investigate the stability of α-helix due to residue 14–18, an MC simulation of 2DX4 by starting from an all-helix conformation is conducted. Because the expanding of the strand affects the size of 2DX4, we record the radius of gyration (R_g) for structure resembling the α-helix. Larger R_g represents structures with extended strands, whereas smaller R_g represents structures that are closer to the standard α-helix. Because each R_g interval may contains several helix structures with different energy values, the internal energy U, defined by the Boltzmann statistics

FIGURE 3 Nearest-neighbor propensity of 2DX4 obtained by statistical analysis of the PDB. Here the dual propensity implies the residue pair can adopt either α- or β-structure. By contrast, the neutral propensity implies that the residue pair is free to rotate in dihedral angles and it is often that a turn region of antiparallel β-sheet is developed.

$$U = \sum_E E \exp(-\beta E),$$

is evaluated as a function of R_g. In Fig. 4, we show the plot of U versus R_g. It is seen that the lowest energy state is not a complete α-helix. In general, hydrogen bonds and long-range dipole energy favor helix structures (23). In the case of 2DX4, nearest-neighbor interactions V_{NP} compete with these helix-favored energies and result in the lowest total energy state with partial helix and partial strand structure. The native α-helix structure found in our MC simulation is identical to results obtained by the experiment (18) and other simulations (21), indicating the credibility of the coarse-grained potentials described in Eq. 1.

To clarify the final fate of α-helix, we perform full MC simulations by starting from the initial state of a straight line with all dihedral angles φ and ψ being equal to 180°. Indeed, the α-helix and β-hairpin-like structures are found to be two configurations with lowest energies and root mean-square deviation of positions being 3.74 Å and 4.40 Å, respectively. Furthermore, similar to the α-helix structure, the β-hairpin also has variants in addition to the standard hairpin structure (see the next subsection for more details). The simulations take 4×10^8 MC steps and ended on either helix or hairpin states. Furthermore, starting from an α-helix at 400 K ($RT = 0.8$ kcal/mol), the α-helix is transformed into a β-sheet and vice versa. All of the transitions occurred successfully in our MC simulations. However, the helix-to-hairpin transition takes 2–10× more MC steps than that for the transition from hairpin to the helix. A hairpin-to-helix transition finished in ~5×10^7 MC steps, where the reverse process took 10^8 MC steps or longer. Although number of MC steps does not reflect the physical folding time quantitatively, qualitatively, the obtained asymmetry of transition probability does suggest that the sheet formation of 2DX4 is a slower process than the formation of helix.

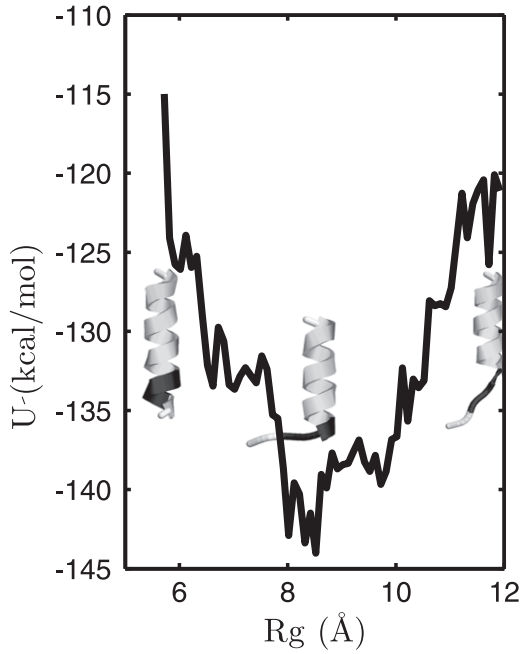

FIGURE 4 Internal energy U versus the radius of gyration R_g for α-like structures. Due to the dangling motion of the strand VHW (marked on *inserted cartoons*) near the C-terminal, the complete helix is not the lowest energy state. (Protein snapshots are drawn by using the graphics software RasMol (40).)

Free energy landscape

To make sure the helix and hairpin structures found in MC simulations are the only two native structures, we calculate the free energy by employing the Wang-Landau algorithm. To characterize the energy landscape, we use the contact ratios Q and Q' as coordinates. Here Q is defined by ratios of contact number of a given state to that of the minimum α-helix structure and Q' is defined similarly with the reference structure being the perfect β-hairpin structure. The free energy F is thus a function of Q and Q', both of which range from 0 to 1. In the calculation, to insure that all regions can be accessed, a trial run with 4×10^8 MC steps is first performed to identify regions with scarce probability. In the latter runs, free energy density in these regions will be computed separately.

Fig. 5 *a* shows the resulting complete free energy landscape for 2DX4. It demonstrates that the free energy has minima at helix and hairpin states. As we can see, similar to the α-helix structure, in addition to the standard hairpin structure, the β-hairpin also has a variant structure labeled by β', whose turn is shifted by one side chain in comparison to that of the hairpin. Both the hairpin β and β' structures have the same contact number Q and the same energy; hence they can be considered collectively as the hairpinlike structures. The difference of free energies for the helix and hairpinlike structures is <0.17 kcal/mol at room temperature, which clearly demonstrates that 2DX4 is a protein with two stable native structures. In Fig. 5 *b*, the one-dimensional free energy curves $F(Q)$ are deduced from the density of states $g(E,Q,Q')$ via the formula

$$\exp\left(\frac{-F(Q)}{k_B T}\right) = \sum_{E,Q'} g(E,Q,Q') \exp\left(\frac{-E}{k_B T}\right).$$

A free-energy barrier at ~10 kcal/mol exists between helix and hairpin structures, Because the energy barrier is much larger than typical energy fluctuations $k_B T$, it stabilizes both the helix and hairpin structures. The free energy landscape also depends on temperature. At temperature $k_B T = 0.8$, ~400 K, the minimum at helix side expands from $Q = 1$ to $Q = 0.65$ with residues 1–10 being kept in helix conformation. In other words, half of the peptide on N-terminal is thermally stable in helix, and residues 11–14 are free to denature at high temperatures.

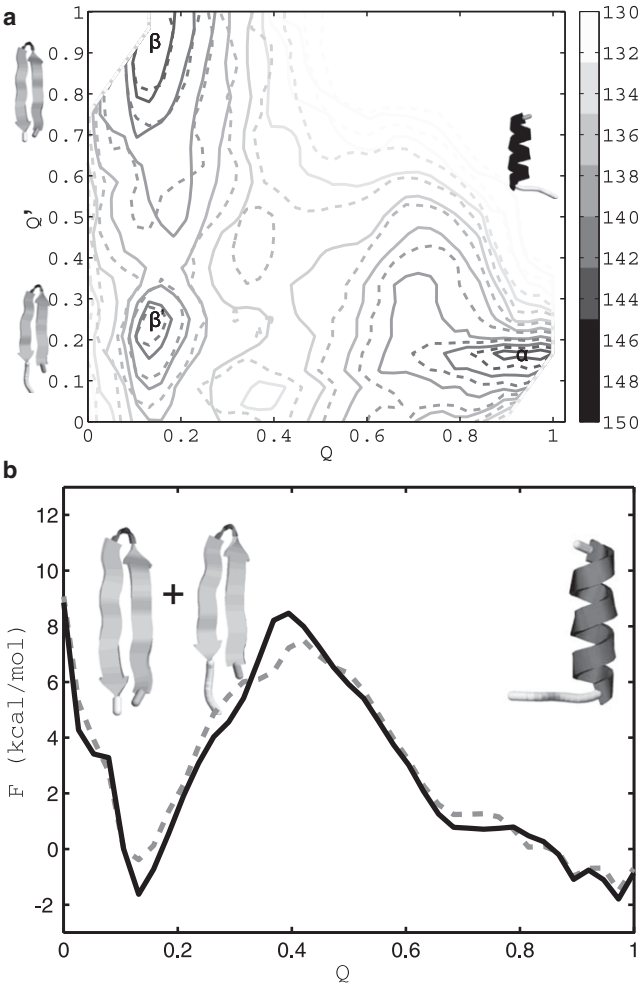

FIGURE 5 (*a*) Free energy contour $F(Q, Q')$ for 2DX4 (*solid lines*) and DP3 (*dashed lines*) at the experimental temperature, 283 K. Here Q and Q' are the contact ratios based on helix and β-hairpin states, respectively. DP3 is a mutated 2DX4–Y12S mutation. Minima with helix and hairpinlike structures labeled by α, β, and β' are exhibited for both cases; however, for DP3, the helix region gets expanded, whereas the hairpin region gets shrunk, indicating that the helix structure is more stable for DP3. (*b*) Free energy versus Q for 2DX4 and DP3. Here both β' and β correspond to the same Q and are hairpinlike structures exhibited as a local minimum in Q. It is seen that the helix structure becomes the most stable structure for DP3, consistent with experiments.

As a comparison, we examine energy landscapes of mutated 2DX4–Y12S mutation, which are labeled as DP3 and DP5 in the previous experiment (18). It is reported that DP3 has zero population of hairpin formation in the sense that even though there is minor intrastrand signal, there is no interstrand signal for the hairpin structure. It is therefore important to examine native structures of DP3 in our model. Fig. 5 *a* reveals that for DP3, the helix region gets expanded, whereas hairpin regions get reduced. This indicates that the helix structure is more stable for DP3. Indeed, Fig. 5 *b* shows that the free energy of the helix state is less than that of the hairpin state by 1.1 kcal/mol at room temperature. In addition, we find that this energy difference is sensitive to temperature and becomes 1.4 kcal/mol at 100 K.

In contrast, for DP5, the free energy of the helix state is found to be fixed at 100–298 K, suggesting that helical structure is thermally more stable in DP5 than in DP3, in agreement with experimental observation (18). Note that it was presumed (18) that absence of π-π interaction of Tyr^{12}-His^{7} near the turn region is the cause for the absence of hairpin in DP3. In addition, the sequence propensity is also relevant. By closely inspecting the neighboring propensity energy E_{NP}, the G11-Y12-I13 peptide has -0.5 kcal/mol and -1.9 kcal/mol in helix and sheet conformations, respectively. In contrast, the G11-S12-I13 peptide in DP3 has -1 kcal/mol and 0 kcal/mol in helix and sheet conformations. Namely, the three successive residues in DP3 have a helical propensity; however, in DP5 these residues have a sheet propensity without losing a helix propensity. These observations are in accordance with experimental results that DP3 has only helical population and DP5 are stable both in helix and sheet conformations.

Mechanism of degeneracy

The mechanism for the existence of degenerate native structures can be explored by analyzing changes of different energy terms when 2DX4 changes between the helix and the hairpin structures. In Fig. 6, we shows changes of different energies along one of the paths that connects the helix and the hairpin structures. Because the route is chosen such that 2DX4 is not fully stretched on the route, the energy changes of the sequence-dependent terms, E_{NP}, E_{MJ}, and E_{SA} are small and may appear to play minor roles during the folding process. Nonetheless, by taking conformation 8 as a example, we find that the total energy is -150 kcal/mol and $E_{NP} + E_{MJ} + E_{SA}$ is -55 kcal/mol. Hence the sequence-dependent energy is 36% of the total energy and plays a major role in the folding. The obtained percentage of the sequence-dependent free energy is generally consistent with experimental observations in which it is explicitly demonstrated that whereas specific proteins, such as protein G and protein L, may have 75% difference in their sequences, the free energy released during folding differs only by ~28% (38,39).

From Fig. 6, it is clear that there is a large compensation between hydrogen-bond energy (HB) and local dipole energy in going from the helix structure to the hairpin structures and vice versa. In the inset of Fig. 6, it is seen that even though there is also a large change of the distribution of E_{NP} between α-propensity (NP^{α}) and β-propensity (NP^{β}), the net change of E_{NP} is small. Hence the main driving mechanism is the compensation between hydrogen bond and the local dipole energy. Physically, it is known that the helix structure has more hydrogen bonds (23) and hence one loses energy in hydrogen bonds by going from the helix structure to the hairpin structure. On the other hand, β-sheets contain

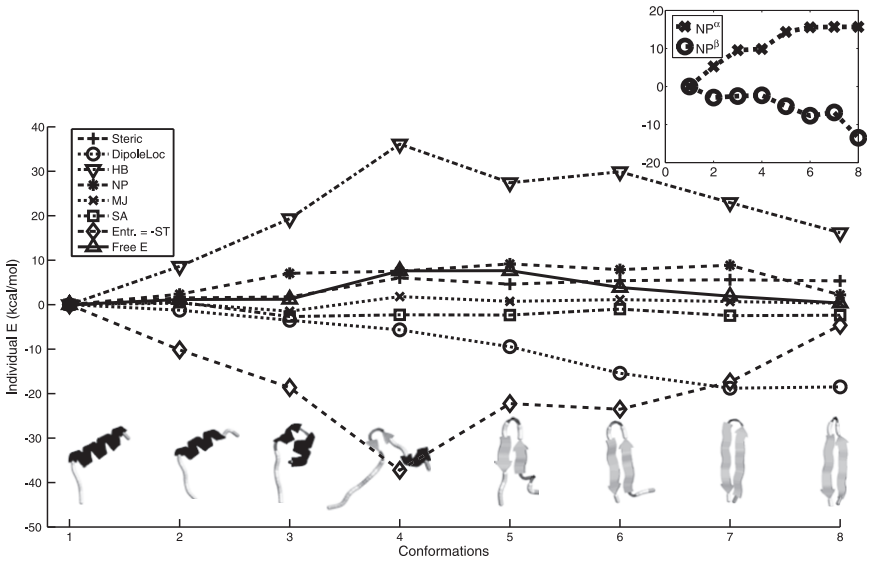

FIGURE 6 Comparison of different energy contributions during the transition between the helix and the hairpinlike structures. (*Inset*) Corresponding change of the distribution of E_{NP} between α-propensity (NP^{α}) and β-propensity (NP^{β}). Here the entropy is defined by $k_B \log [g(E,Q)]$. Large compensation between hydrogen-bond energy (HB) and local dipole energy indicates that the compromising of HB and local dipole energy creates the degenerate native states.

large antiparallel dipoles on nearest-neighboring amide planes, which lowers the local dipole interaction energy. The competition of hydrogen-bond energy and local dipole energy depends on the length of the protein.

To see why 2DX4 is special, we examine the difference of hydrogen-bond energy and local dipole energy for α-helix and β-sheet versus number of side chains. The energy difference is optimized with respect to the number of β-strands. Fig. 7 shows the computed optimized difference of hydrogen-bond energy and local dipole energy for α-helix and β-sheet versus number of side chains. It is seen that the difference of hydrogen-bond energy and local dipole energy vanishes at number of side chains being around 18 amino acids, which is precisely the number of side chains in 2DX4 Therefore, our results show that although differences in other energy changes in 2DX4 contribute 2–3 kcal/mol, the major compensation in energy comes from the hydrogen-bond energy and local dipole energy and it leads to the degeneracy of the helix and hairpin structures.

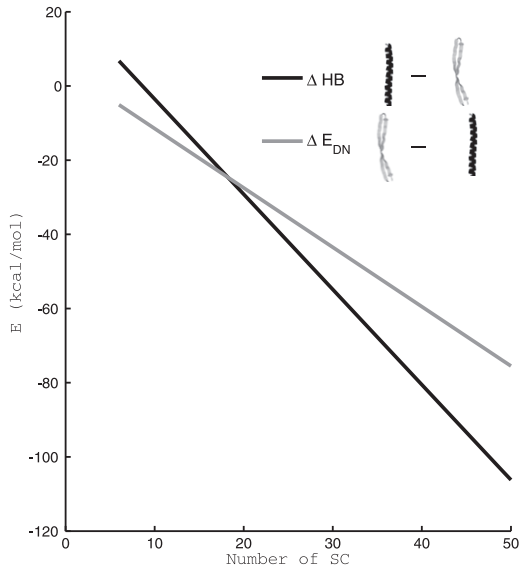

FIGURE 7 Difference of hydrogen-bond energy and local dipole energy for α-helix and β-sheet versus the number of side chains. It is seen that the difference of hydrogen-bond energy and local dipole energy vanishes at the number of side chains being around 18 amino acids.

DISCUSSION AND CONCLUSION

In conclusion, the possibility for the existence of degenerate native states provides what to our knowledge is new insight into the folding mechanism of proteins. Our results show that the possibility is realized in the designed 2DX4, which possesses two nearly degenerate native structures: one has a helix structure, whereas the other has a hairpinlike structure. The two degenerate native structures of 2DX4 are shown to be separated by an energy barrier of 10 kcal/mol. Based on the usage of the Arrhenius form for the kinetic rate, $k = Ae^{-E/k_BT}$, where the preexponential factor A is the attempt rate and can be estimated as inverse of typical fold time, 10^3/s, we find that the kinetic rate for the transformation between two native states is ~6×10^{-5}/s. The transformation rate is thus a slow process. As a result, two degenerate structures are stabilized, consistent with experiments (18) in which no apparent transitions between two degenerate structures are observed.

Our results further indicate that the existence of two degenerate native structures in 2DX4 is driven by large compensation between the hydrogen-bond energy and the local dipole energy. The length study of the difference between hydrogen-bond energy and local dipole energy for α-helix and β-hairpin shows that 2DX4 is special in that it has 18 amino acids, which is exactly the number required for balancing the hydrogen-bond energy and local

dipole energy. Therefore, although differences of other energy terms in 2DX4 do contribute, the major energy compensation in going from α-helix and β-hairpin is determined by the hydrogen-bond energy and local dipole energy, which leads to the observed degeneracy of the helix and hairpin structures. If the length study is further extended to larger number of side chains, we find that the next balance between hydrogen-bond energy and local dipole energy for α-helix and β-sheet could occur for the number of side chains being ~40. Although it does not mean that degenerate binary native structures will necessarily occur, our results provide important clues for the study of native structures of proteins, especially for proteins with possibly degenerate native states.

SUPPORTING MATERIAL

One figure is available at http://www.biophysj.org/biophysj/supplemental/S0006-3495(12)00582-6.

We thank Prof. Chia-Ching Chang for helpful discussions.

This work was supported by the National Science Council and National Tsing Hua University of Taiwan.

REFERENCES

1. Anfinsen, C. B. 1973. Principles that govern the folding of protein chains. *Science.* 181:223–230.
2. Hamada, D., S. Segawa, and Y. Goto. 1996. Non-native α-helical intermediate in the refolding of β-lactoglobulin, a predominantly β-sheet protein. *Nat. Struct. Biol.* 3:868–873.
3. Kuwata, K., M. Hoshino, …, Y. Goto. 1998. $\alpha \rightarrow \beta$ transition of β-lactoglobulin as evidenced by heteronuclear NMR. *J. Mol. Biol.* 283: 731–739.
4. Zhang, S., K. Iwata, …, J. P. Lee. 2000. The Alzheimer's peptide Aβ adopts a collapsed coil structure in water. *J. Struct. Biol.* 130:130–141.
5. Serpell, L. C. 2000. Alzheimer's amyloid fibrils: structure and assembly. *Biochim. Biophys. Acta.* 1502:16–30.
6. Sticht, H., P. Bayer, …, P. Rösch. 1995. Structure of amyloid A4-(1-40)-peptide of Alzheimer's disease. *Eur. J. Biochem.* 233:293–298.
7. Coles, M., W. Bicknell, …, D. J. Craik. 1998. Solution structure of amyloid β-peptide(1-40) in a water-micelle environment. Is the membrane-spanning domain where we think it is? *Biochemistry.* 37:11064–11077.
8. Xu, Y., J. Shen, …, H. Jiang. 2005. Conformational transition of amyloid β-peptide. *Proc. Natl. Acad. Sci. USA.* 102:5403–5407.
9. Cerpa, R., F. E. Cohen, and I. D. Kuntz. 1996. Conformational switching in designed peptides: the helix/sheet transition. *Fold. Des.* 1:91–101.
10. Zhang, S., and A. Rich. 1997. Direct conversion of an oligopeptide from a β-sheet to an α-helix: a model for amyloid formation. *Proc. Natl. Acad. Sci. USA.* 94:23–28.
11. Murayama, K., and M. Tomida. 2004. Heat-induced secondary structure and conformation change of bovine serum albumin investigated by Fourier transform infrared spectroscopy. *Biochemistry.* 43:11526–11532.
12. Montserret, R., M. J. McLeish, …, F. Penin. 2000. Involvement of electrostatic interactions in the mechanism of peptide folding induced by sodium dodecyl sulfate binding. *Biochemistry.* 39:8362–8373.
13. Kabsch, W., and C. Sander. 1984. On the use of sequence homologies to predict protein structure: identical pentapeptides can have completely different conformations. *Proc. Natl. Acad. Sci. USA.* 81: 1075–1078.
14. Cohen, B. I., S. R. Presnell, and F. E. Cohen. 1993. Origins of structural diversity within sequentially identical hexapeptides. *Protein Sci.* 2:2134–2145.
15. Minor, Jr., D. L., and P. S. Kim. 1996. Context-dependent secondary structure formation of a designed protein sequence. *Nature.* 380: 730–734.
16. Cordes, M. H., R. E. Burton, …, R. T. Sauer. 2000. An evolutionary bridge to a new protein fold. *Nat. Struct. Biol.* 7:1129–1132.
17. Alexander, P. A., Y. He, …, P. N. Bryan. 2009. A minimal sequence code for switching protein structure and function. *Proc. Natl. Acad. Sci. USA.* 106:21149–21154.
18. Araki, M., and A. Tamura. 2007. Transformation of an α-helix peptide into a β-hairpin induced by addition of a fragment results in creation of a coexisting state. *Proteins.* 66:860–868.
19. Bernstein, F. C., T. F. Koetzle, …, M. Tasumi. 1978. The Protein Data Bank: a computer-based archival file for macromolecular structures. *Arch. Biochem. Biophys.* 185:584–591.
20. Duan, Y., and P. A. Kollman. 1998. Pathways to a protein folding intermediate observed in a 1-microsecond simulation in aqueous solution. *Science.* 282:740–744.
21. Itoh, S. G., A. Tamura, and Y. Okamoto. 2010. Helix-hairpin transitions of a designed peptide studied by a generalized-ensemble simulation. *J. Chem. Theory Comput.* 6:979–983.
22. Klimov, D. K., and D. Thirumalai. 2000. Mechanisms and kinetics of β-hairpin formation. *Proc. Natl. Acad. Sci. USA.* 97:2544–2549.
23. Chen, N.-Y., Z.-Y. Su, and C.-Y. Mou. 2006. Effective potentials for folding proteins. *Phys. Rev. Lett.* 96:078103.
24. Miyazawa, S., and R. Jernigan. 1985. Estimation of effective interresidue contact energies from protein crystal structures: quasi-chemical approximation. *Macromolecules.* 18:534–552.
25. Miyazawa, S., and R. L. Jernigan. 1996. Residue-residue potentials with a favorable contact pair term and an unfavorable high packing density term, for simulation and threading. *J. Mol. Biol.* 256: 623–644.
26. Irbäck, A., and F. Sjunnesson. 2004. Folding thermodynamics of three β-sheet peptides: a model study. *Proteins.* 56:110–116.
27. Kortemme, T., A. V. Morozov, and D. Baker. 2003. An orientation-dependent hydrogen bonding potential improves prediction of specificity and structure for proteins and protein-protein complexes. *J. Mol. Biol.* 326:1239–1259.
28. Chaikin, P. M., and T. C. Lubensky. 1995. Principles of Condensed Matter Physics, 1st ed. Cambridge University Press, Cambridge, UK.
29. Cheung, M. S., A. E. García, and J. N. Onuchic. 2002. Protein folding mediated by solvation: water expulsion and formation of the hydrophobic core occur after the structural collapse. *Proc. Natl. Acad. Sci. USA.* 99:685–690.
30. Shimizu, S., and H. S. Chan. 2001. Configuration-dependent heat capacity of pairwise hydrophobic interactions. *J. Am. Chem. Soc.* 123:2083–2084.
31. Dias, C. L., M. Karttunen, and H. S. Chan. 2011. Hydrophobic interactions in the formation of secondary structures in small peptides. *Phys. Rev. E.* 84:041931.
32. Betancourt, M. R., and J. Skolnick. 2001. Finding the needle in a haystack: educing native folds from ambiguous ab initio protein structure predictions. *J. Comput. Chem.* 22:339–353.
33. Wang, F., and D. P. Landau. 2001. Efficient, multiple-range random walk algorithm to calculate the density of states. *Phys. Rev. Lett.* 86:2050–2053.
34. Rathore, N., T. A. Knotts, and J. J. de Pablo. 2003. Density of states simulations of proteins. *J. Chem. Phys.* 118:4285–4290.
35. Ojeda, P. A., A. Londono, …, M. Garcia. 2008. Monte Carlo simulations of proteins in cages: influence of confinement on the stability of intermediate states. *Biophys. J.* 96:1076–1082.

36. Betancourt, M. R., and J. Skolnick. 2004. Local propensities and statistical potentials of backbone dihedral angles in proteins. *J. Mol. Biol.* 342:635–649.

37. Matsuo, Y., and K. Nishikawa. 1994. Protein structural similarities predicted by a sequence-structure compatibility method. *Protein Sci.* 3:2055–2063.

38. McCallister, E. L., E. Alm, and D. Baker. 2000. Critical role of β-hairpin formation in protein G folding. *Nat. Struct. Biol.* 7:669–673.

39. Kim, D. E., C. Fisher, and D. Baker. 2000. A breakdown of symmetry in the folding transition state of protein L. *J. Mol. Biol.* 298:971–984.

40. Sayle, R. A., and E. J. Milner-White. 1995. RASMOL: biomolecular graphics for all. *Trends Biochem. Sci.* 20:374–376.